J Intell Robot Syst (2018) 89:175–189
DOI 10.1007/s10846-017-0544-3

Effective Turning Motion Control of Internally Actuated Autonomous Underwater Vehicles

Saeedeh Ziaeefard · Brian R. Page · Anthony J. Pinar · Nina Mahmoudian

Received: 29 June 2016 / Accepted: 17 March 2017 / Published online: 8 April 2017

Abstract This paper presents a novel roll mechanism and an efficient control strategy for internally actuated autonomous underwater vehicles (AUVs). The developed control algorithms are tested on Michigan Tech's custom research glider, ROUGHIE (Research Oriented Underwater Glider for Hands-on Investigative Engineering), in a controlled environment. The ROUGHIE's design parameters and operational constraints were driven by its requirement to be man portable, expandable, and maneuverable in shallow water. As an underwater glider, the ROUGHIE is underactuated with direct control of only depth, pitch, and roll. A switching control method is implemented on the ROUGHIE to improve its maneuverability, enabling smooth transitions between different motion patterns. This approach uses multiple feedforward-feedback controllers. Different aspects of the roll mechanism and the effectiveness of the controller on turning motion are discussed based on experimental results. The results illustrate that the ROUGHIE is capable of achieving tight turns with a radius of 2.4 meters in less than 3 meters of water, or one order of magnitude improvement on existing internally actuated platforms. The developed roll mechanism is not specific to underwater gliders and is applicable to all AUVs, especially at lower speeds and in shallower water when external rudder is less effective in maneuvering the vehicle.

Keywords Underactuated robot · Marine robot · Maneuverability · Motion control · Underwater glider · Internal actuation

This work is funded in part by Office of Naval Research grant No. N00014-15-1-2599 and National Science Foundation grant No. 1453886.

S. Ziaeefard · B. R. Page · N. Mahmoudian (✉)
Department of Mechanical Engineering-Engineering Mechanics, Michigan Technological University, Houghton, MI, USA
e-mail: ninam@mtu.edu

S. Ziaeefard
e-mail: sziaeefa@mtu.edu

B. R. Page
e-mail: bpage@mtu.edu

A. J. Pinar
Department of Electrical and Computer Engineering, Michigan Technological University, Houghton, MI, USA
e-mail: ajpinar@mtu.edu

1 Introduction

In the past decade, Autonomous Underwater Vehicle (AUV) development has reached technical maturity. AUVs are used on several different types of missions ranging from long endurance oceanographic missions [24] to intervention missions [15], and surveillance [17, 20].

Although some AUVs are fully actuated or over actuated such as the Delphin2 [14], the majority of AUVs are underactuated. One standard configuration of these underactuated AUVs includes a stern thruster and pair of rudders to control pitch and yaw while in motion such as [2–4, 18].

Underwater Gliders (UGs) are an extremely efficient subclass of AUV that travel through the water in what is known as a sawtooth pattern. The sawtooth pattern in gliders arises due to the locomotive method used–gliders travel through the water column powered by a buoyancy drive rather than traditional propellers or jets. The buoyancy drive can take different forms, but all involve adjusting the net buoyancy of the vehicle to be slightly positive or slightly negative, inducing a vertical motion. A wing translates this vertical motion into forward motion.

Typical gliders such as Slocum [21], Spray [19] and Seaglider [7], known as legacy gliders, are equipped with internal mass control actuators, though some Slocum have external rudders for heading control. Gliders with exclusive internal actuation are constrained to three of their six degrees of freedom (depth/heave, pitch, and roll), making navigation of these underactuated vehicles challenging.

The main limitation of UGs in practical scenarios is maneuverability. A series of numerical and analytical studies on UG maneuverability investigate steady turn solutions using stability and performance analysis [8, 12, 22, 23].

These studies motivated the Nonlinear and Autonomous Systems Lab (NAS Lab) at Michigan Tech to develop the Research Oriented Underwater Glider for Hands-on Investigative Engineering (ROUGHIE) [13], shown in Fig. 1.

Although the ROUGHIE is underactuated, the use of a novel internal rotary mechanism [25] and efficient motion controller allows the ROUGHIE to improve maneuverability by achieving tight turns. To the best of the authors' knowledge, the ROUGHIE is the most maneuverable internally actuated underwater glider, capable of a turn radius down to 2.4 meters for a 1.2 meter vehicle in 3 meters depth of water [13, 25]. The ROUGHIE's 2.4 meter turn radius is an order of magnitude improvement over the typical 30-50 meter turn radii for internally actuated underwater gliders [6, 10, 22]. The roll mechanism and control architecture developed for the ROUGHIE can also be extended to more traditional AUV, especially at low speed and in shallow water when external rudder is not as effective.

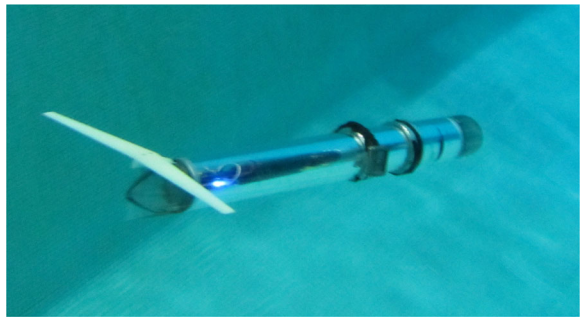

Fig. 1 The Research Oriented Underwater Glider for Hands-on Investigative Engineering (ROUGHIE) is a capable low-cost underwater glider. It is approximately 1.2 meters long and weighs 12.8 kg making it easily portable by one person

The remainder of this paper discusses the ROUGHIE design overview in Section 2, kinematic analysis in Section 3, control development in Section 4, results in Section 5, and conclusions and future work in Section 6.

2 Design Overview

The ROUGHIE is designed around a modular, rail based layout consisting of three actuated modules and a processing module. The modular layout enables field modification and upgrades with minimal tools, easy experimentation with new systems, and internal organization. Each of the modules interfaces with a common mounting rail that serves as eccentric rotary mass, cable guide, and structural support to the glider.

Starting from the front of the ROUGHIE is the roll module that affects the vehicle roll angle through internal actuation of the common rail about the vehicle longitudinal axis. The roll module, Fig. 2a, consists of a machined aluminum ring that interfaces the internal hull surface to a servo with a concentrically mounted shaft. Through this shaft, the servo is attached to the common rail. This common rail carries approximately 90% of the vehicle's internal mass. By rolling the common rail, ROUGHIE's center of gravity shifts along the lateral axis of the vehicle (port/starboard), causing the vehicle itself to roll.

The current system is capable of rolling the internal rail $+/-$ 70 degrees and is only limited by the

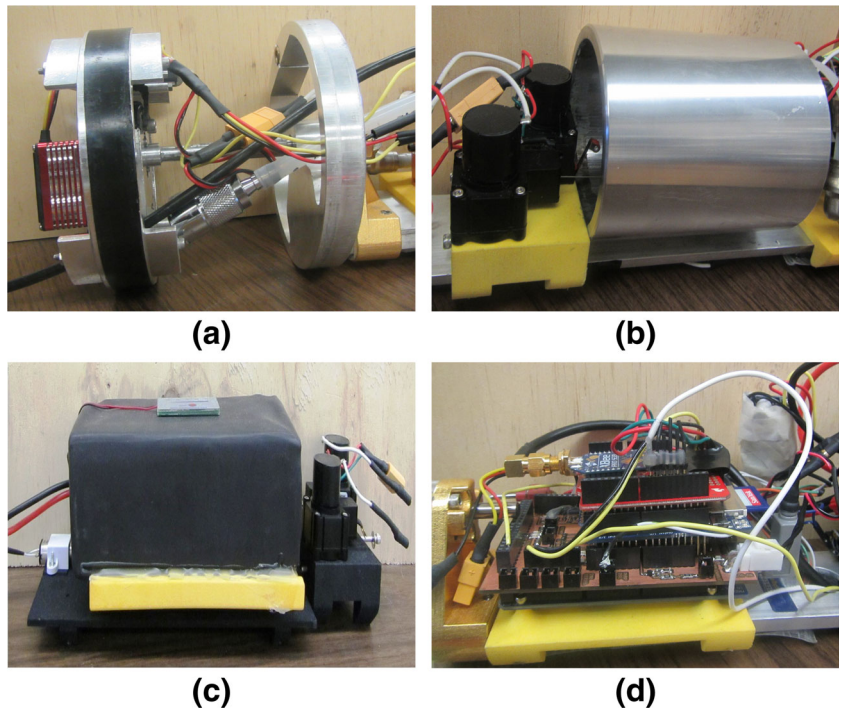

Fig. 2 (**a**) The roll module interfaces the system rail (right side) to the vehicle hull (not shown). (**b**) The buoyancy module actuates the net buoyancy slightly positive or negative and is the locomotive source for the glider. (**c**) The pitch module drives the system battery fore and aft in the vehicle slightly shifting center of gravity and causing pitching moments. (**d**) The processing module contains the electronics stack with microprocessor and associated breakouts to control the electromechanical devices in ROUGHIE

configuration of the other modules. In water this results in rolling in excess of 60 degrees with our current trimming solution.

Aft of this module is the buoyancy module that controls ballast amount and thus vehicle vertical velocity in the water column as well as contributing to the vehicle pitch angle. The buoyancy module, Fig. 2b, consists of two 3D printed mounting parts, a machined ballast tank, a normally closed solenoid valve, and a water pump. One of the 3D printed mounting parts supports the pump and plumbing, while the other supports the ballast tank and two draw wire sensors used to provide position feedback of the ballast piston and the pitch mass.

Further back is the pitch module that shifts a mass linearly to perform small pitching motions. Figure 2c shows the pitch module. This module consists of a 3D printed base plate and control plate that provide structure and mounting to the other parts as well as the system battery that rides atop the control plate. The remaining components include a linear bearing, power screw, and micro gearmotor which all contribute to low friction actuation of the pitch motion. This system is able to actuate the 2.2 kg battery through 8.5 cm of motion.

At the rear of the ROUGHIE is the processing module that performs all computation, control, and data logging. The processing module, shown in Fig. 2d, consists of a 3D printed mounting platform that rigidly supports the central processor and associated electronics. In the current revision of the ROUGHIE, the central processor is an Arduino Mega. The use of a standard hobby level processor makes the ROUGHIE accessible to new researchers and easily expandable. The processing module also contains a custom circuit board to interface the Arduino with the peripheral electromechanical components, as well as two off-the-shelf expansion shields providing wireless communication and data logging.

Similar to the mechanical system in ROUGHIE, the electrical system has also been designed to be as modular as possible. This approach results in an electrical setup that is easy to diagnose and upgrade, since most components can be easily replaced through the use of friction locking connectors and off-the-shelf electronic solutions. The main wire harness is managed via a dedicated track running the length of the underside of the mounting rail, preventing the wires from interfering with the system's moving parts.

Enclosing the modules is the vehicle hull and external surfaces. The ROUGHIE has two hull configurations: a clear acrylic hull for low pressure tests to ease debugging, and an aluminum hull for higher pressure tests up to 30 meters. The front and rear end caps are designed for hydrodynamic efficiency and the rear mounted wing is of a NACA-0012 profile to provide equal lift in both up and down glides.

3 Kinematics

To understand the kinematics of the ROUGHIE, we model this vehicle as a system of mass blocks per [9]. This system is composed of a linear sliding mass block (m_s), a common rail rotary mass (m_r), a buoyancy mass (m_b), and a glider hull mass (m_h). We establish three reference frames (Fig. 3) to describe the dynamics of the ROUGHIE. The *inertial frame* (x, y, z) is fixed on the earth in the North-East-Down direction. The *body frame's* (x_b, y_b, z_b) origin is located at the glider's center of buoyancy with its $x-$direction along the vehicle's longitudinal axis, its y-direction in the starboard direction, and the $z-$direction points downward. The *flow frame* is defined relative to the body frame by rotating the body frame around the $y-axis$ and $z-axis$ via the rotation matrix

$$\mathbf{R}_{bf} = \begin{bmatrix} \cos(\alpha)\cos(\beta) & -\cos(\alpha)\sin(\beta) & -\sin(\alpha) \\ \sin(\beta) & \cos(\beta) & 0 \\ \sin(\alpha)\cos(\beta) & -\sin(\alpha)\sin(\beta) & \cos(\alpha) \end{bmatrix}; \tag{1}$$

where α and β are glider's angle of attack and sideslip angle, respectively. We define the angle of attack, α, and sideslip angle, β, to satisfy

$$\tan(\alpha) = \frac{w}{u} \tag{2}$$

$$\sin(\beta) = \frac{u}{\sqrt{u^2+v^2+w^2}}, \tag{3}$$

where u, v, and w are the glider's translational velocities in the body frame (x_b, y_b, z_b). Figure 3 illustrates the mechanics of the mass system and the reference frames, and Table 1 summarizes the notation used in this section.

We must derive the total kinetic energy of the glider system to get the total dynamic model of the glider. The total kinetic energy of the glider system is the cumulative of each mass block's kinetic energy,

$$T_t = T_{ms} + T_{mb} + T_{mr} + T_{mh}, \tag{4}$$

where T_{ms}, T_{mb}, T_{mr}, and T_{mh} represent the kinetic energy of the sliding mass, buoyancy mass, rotary mass, and glider hull mass, respectively.

The kinetic energy of the sliding mass expressed as

$$T_{ms} = \frac{1}{2} m_s ||\mathbf{V}_s||^2 + \frac{1}{2} \mathbf{\Omega}_s^T \mathbf{I}_s \mathbf{\Omega}_s, \tag{5}$$

where $\mathbf{I}_s$ is the inertia of the sliding mass and $\mathbf{\Omega}_s$ is the angular velocity in body frame, since the sliding mass is bound to one degree of freedom in longitudinal axes. The remaining terms are

$$\mathbf{V}_s = \mathbf{V} - \mathbf{r}_s \times \mathbf{\Omega}, \tag{6}$$

$$\mathbf{\Omega}_s = \mathbf{\Omega}, \tag{7}$$

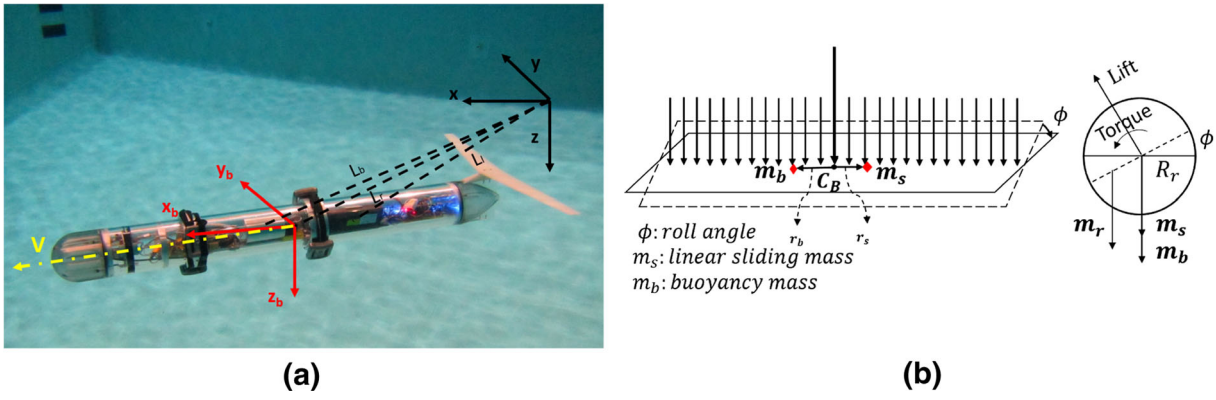

Fig. 3 Reference frames and mass system distribution

Table 1 Notation

Notation	Definition
m_s	Linear sliding mass block
m_r	Common rail rotary mass
m_b	Buoyancy mass
m_h	Glider hull mass
(x, y, z)	Inertial reference frame
(x_b, y_b, z_b)	Body reference frame
$\mathbf{R}_{bf}$	Rotation matrix transforming from the body frame to the flow frame
α	Attack angle
β	Sideslip angle
$\mathbf{V} = [u, v, w]^T$	Translational velocity in the body frame
T_t	Total kinetic energy of glider system
T_{ms}	Kinetic energy of sliding mass
T_{mb}	Kinetic energy of buoyancy mass
T_{mr}	Kinetic energy of rotary mass
T_{mh}	Kinetic energy of hull mass
$\mathbf{V}_s$	Linear mass block velocity
$\boldsymbol{\Omega}_s$	Angular velocity of sliding mass in the body frame
$\mathbf{I}_s$	Inertia of sliding mass
$\mathbf{r}_s$	Position of sliding linear mass in body frame
$\boldsymbol{\Omega} = [p \quad q \quad r]^T$	Vehicle angular velocity in body frame
$\mathbf{V}_b$	Buoyancy mass block velocity
$\boldsymbol{\Omega}_b$	Angular velocity of buoyancy mass in the body frame
$\mathbf{I}_b$	Inertia of buoyancy mass
$\mathbf{r}_b$	Position of buoyancy mass in body frame
$\mathbf{r}_r$	Position of rotary mass in body frame
r_{rx}	Position of rail in $x-$ direction
$(\hat{\mathbf{x}}, \hat{\mathbf{y}}, \hat{\mathbf{z}})$	Standard basis for inertial reference frame
R_r	Roll mass semi-circular eccentric radius
γ	Vehicle internal roll angle
$\boldsymbol{\Omega}_r$	Angular velocity of roll mass in the body frame
$\mathbf{I}_r$	Inertia of roll mass
$\mathbf{R}_x$	Rotational matrix along longitudinal axis in body frame
$\mathbf{M}_A$	Added mass
$\mathbf{I}_A$	Added inertia matrix
$\mathbf{C}_A$	Cross term in $\mathbf{M}$ depending on the surrounding fluid in the body frame
$\mathbf{M}$	Added mass
$\mathbf{p}$	Translational momentum
$\mathbf{q}$	Angular momentum
$\mathbf{F}_{ext}$	External force applied to the vehicle in the flow frame
$\mathbf{T}_{ext}$	External momentum of the vehicle in the flow frame
m	Displaced water mass to calculate net buoyancy
g	Gravitational force constant
$\hat{\mathbf{k}}$	Unit vector points to the gravitational force direction (downwards)
$\mathbf{L}_r$	Distance from the roll mass' center of gravity to the center of inertia frame

Table 1 (continued)

Notation	Definition
$\mathbf{L}_b$	Distance from the buoyancy mass' center of gravity to the center of inertia frame
$\mathbf{L}_l$	Distance from the linear sliding mass' center of gravity to the center of inertia frame
$\mathbf{F}_h$	Hydrodynamic force
$\mathbf{T}_h$	Hydrodynamic torque
$\mathbf{R}_{ib}$	Rotation matrix mapping the inertial frame to body frame
$\mathbf{b}$	Vehicle position in inertia frame
$\boldsymbol{\nu} = [\mathbf{V}^T \quad \boldsymbol{\Omega}^T]$	Generalized translational and angular velocity in body frame
$\boldsymbol{\mu} = [\mathbf{P}^T \quad \mathbf{Q}^T]$	Generalized translational and angular momentum in body frame
R_t	Turn radius of glider
ω_3	Angular velocity of glider along a circular helix
ϕ	Vehicle roll angle
θ	Vehicle pitch angle
ψ	Vehicle yaw angle

where $\mathbf{V} = [u, v, w]^T$ is glider's translational velocity in the body frame. and $\boldsymbol{\Omega} = [p \quad q \quad r]^T$ is the angular velocity in the body frame.

The net buoyancy is controlled by a pump that pumps water into and out of a ballast tank, changing the buoyancy mass. The kinetic energy of the buoyancy mass can be expressed as

$$T_{mb} = \frac{1}{2} m_b ||\mathbf{V}_b||^2 + \frac{1}{2} \boldsymbol{\Omega}_b^T \mathbf{I}_b \boldsymbol{\Omega}_b, \tag{8}$$

where $\mathbf{I}_b$ is inertia of the buoyancy mass in the form of a cylinder whose length varies depending on the buoyancy mass changes through different stages of the glide; $\mathbf{I}_b$ is fixed during turning motion, and since the buoyancy mass is fixed on the common rail,

$$\mathbf{V}_b = \mathbf{V} - \mathbf{r}_b \times \boldsymbol{\Omega}, \tag{9}$$

$$\boldsymbol{\Omega}_b = \boldsymbol{\Omega}. \tag{10}$$

The rotary mass, i.e., the common rail and all the attached modules comprising 90% of the glider's internal mass, pivots around the longitudinal axis of the glider. The position of the rotary mass' center of gravity is

$$\mathbf{r}_r = r_{rx}\mathbf{x}_b + R_r(\cos(\gamma + \pi/2))\mathbf{y}_b + \sin(\gamma + \pi/2)\mathbf{z}_b), \tag{11}$$

where γ is the internal roll angle, or servo angle. r_{rx} is the position of the rail in x-direction which does not vary since the common rail is only constrained to rotate about the $x-$axis, thus the kinetic energy of the ROUGHIE due to the rotary mass is only dependent on γ.

The kinetic energy of the rotary mass, m_r, is

$$T_{mr} = \frac{1}{2} \boldsymbol{\Omega}_r^T \mathbf{I}_r(\gamma) \boldsymbol{\Omega}_r, \tag{12}$$

where $\boldsymbol{\Omega}_r$ is the angular velocity of the common rail induced by the servo and $\mathbf{I}_r(\gamma)$ is the symmetric inertia matrix of the roll mass defined as

$$\mathbf{I}_r(\gamma) = \mathbf{R}_x^T(\gamma) \mathbf{I}_r(0) \mathbf{R}_x(\gamma); \tag{13}$$

$\mathbf{I}_r(\gamma)$ is modeled as a semi-cylinder with the same length as the common rail. $\mathbf{R}_x$ is the rotation matrix along longitudinal axes of the glider in the body frame

$$\mathbf{R}_x = \begin{bmatrix} 1 & 0 & 0 \\ 0 & \cos(\gamma) & -\sin(\gamma) \\ 0 & \sin(\gamma) & \cos(\gamma) \end{bmatrix} \tag{14}$$

Equations 12 and 13 illustrate the effects of the rotary mass on spiraling and turning motion of the vehicle. When the common rail rotates, the roll angle of the glider changes which induces a change in the inertia of the rotary mass and the kinetic energy of the glider. In essence, the turn motion of the ROUGHIE is controlled by the roll angle.

The kinetic energy of the glider due to its hull shape and mass is dependent on the added mass, $\mathbf{M}_A$, added inertia matrix, $\mathbf{I}_A$, and the cross term, $\mathbf{C}_A$, in the body frame due to the surrounding fluid. It is expressed as

$$T_{mh} = \frac{1}{2} \boldsymbol{\nu}^T \mathbf{M} \boldsymbol{\nu} \tag{15}$$

where according to [11]

$$\mathbf{M} = \begin{bmatrix} \mathbf{M}_A & \mathbf{C}_A \\ \mathbf{C}_A^T & \mathbf{I}_A \end{bmatrix}. \tag{16}$$

In these expressions, $\mathbf{M}_A$, $\mathbf{I}_A$, and $\mathbf{C}_A$ are diagonal and are approximated using the strip theory following [23].

According to Newton's second law, the rate of change of momentum of a body is equal to the forces applied to it. Hence the translational momentum rate, $\dot{\mathbf{p}}$, and angular momentum rate, $\dot{\mathbf{q}}$, of the glider in the inertial frame can be expressed as

$$\dot{\mathbf{p}} = \mathbf{F}_{ext} + (m_h + m_b + m_r + m_s - m)g\hat{\mathbf{k}}; \tag{17}$$

$$\dot{\mathbf{q}} = \mathbf{T}_{ext} + \mathbf{L}_r \times m_r g\hat{\mathbf{k}} + \mathbf{L}_b \times m_b g\hat{\mathbf{k}} + \mathbf{L}_l \times m_s g\hat{\mathbf{k}}. \tag{18}$$

Here, $\mathbf{L}_r$, $\mathbf{L}_b$, and $\mathbf{L}_l$ are the distances from the roll mass, buoyancy mass, and linear sliding mass' center of gravity to the center of inertia frame as depicted in Fig. 3, and $\hat{\mathbf{k}}$ is the unit vector pointing downward in the gravity direction. If $\mathbf{P}$ and $\mathbf{Q}$ are the translational and angular momentum of the glider in body frame, the relationship between them with p and q, their counter part in inertial frame, is as follows

$$\mathbf{p} = \mathbf{R}_{ib}\mathbf{P}, \tag{19}$$

$$\mathbf{q} = \mathbf{R}_{ib}\mathbf{Q} + \mathbf{b} \times \mathbf{p}, \tag{20}$$

where $\mathbf{R}_{ib}$ is the rotation matrix that maps the inertial frame to body frame. $\mathbf{F}_{ext}$ and $\mathbf{T}_{ext}$ are the external force and momentum, respectively, applied on the vehicle in the flow frame, expressed as

$$\mathbf{F}_{ext} = \mathbf{R}_{bf}\mathbf{F}_h, \quad \mathbf{T}_{ext} = \mathbf{R}_{bf}\mathbf{T}_h, \tag{21}$$

where $\mathbf{F}_h = [-D \quad SF \quad -L]^T$ and $\mathbf{T}_h = [T_{DL1} \quad T_{DL2} \quad T_{DL3}]^T$, which are the hydrodynamic force and moment, respectively. According to [5], the hydrodynamic coefficients depend on the vehicle velocity, angle of attack, and sideslip angle as

$$D = (K_{D0} + K_D\alpha^2)V^2, \tag{22}$$

$$L = (K_{L0} + K_L\alpha^2)V^2 \tag{23}$$

$$SF = K_\beta\beta V^2, \tag{24}$$

$$T_{DL1} = (K_{MR}\beta + K_P p)V^2, \tag{25}$$

$$T_{DL2} = (K_{M0} + K_M\alpha + K_q q)V^2, \tag{26}$$

$$T_{DL3} = (K_{MY}\beta + K_r r)V^2, \tag{27}$$

$$\tag{28}$$

where $V = ||\mathbf{V}||$ and the K coefficients are the hydrodynamic coefficients of the glider illustrated in Table 2. Since we have not completed an empirical parameter study of the ROUGHIE, these values are borrowed from the Slocum glider due to its similar shape [1].

We define $\boldsymbol{\nu} = [\mathbf{V} \quad \boldsymbol{\Omega}]^T$ as generalized translational and angular velocity and $\boldsymbol{\mu} = [\mathbf{P} \quad \mathbf{Q}]^T$ as generalized translational and angular momentum, both in body frame. The relationship between the vehicle velocity and momentum is expressed as

$$\boldsymbol{\mu} = \mathbf{M}\boldsymbol{\nu}, \tag{29}$$

where $\mathbf{M}$ is the generalized inertial matrix of the glider system given in (16). By differentiating (29) with respect to time we obtain

$$\dot{\boldsymbol{\mu}} = \dot{\mathbf{M}}\boldsymbol{\nu} + \mathbf{M}\dot{\boldsymbol{\nu}}. \tag{30}$$

Thus, to derive the dynamic model of the glider we need to calculate

$$\dot{\boldsymbol{\nu}} = \mathbf{M}^{-1}(\dot{\boldsymbol{\mu}} - \dot{\mathbf{M}}\boldsymbol{\nu}). \tag{31}$$

Substitution yields

$$\dot{\boldsymbol{\nu}} = \mathbf{M}^{-1}\left\{ -\mathbf{M}\boldsymbol{\nu} + \begin{bmatrix} \mathbf{P} \times \boldsymbol{\Omega} \\ \mathbf{Q} \times \boldsymbol{\Omega} + \mathbf{P} \times \mathbf{V} \end{bmatrix} + \begin{bmatrix} m_b g(\mathbf{R}_{ib})^T\hat{\mathbf{k}}) \\ (m_r\mathbf{r}_r + m_s\mathbf{r}_s + m_b\mathbf{r}_b)g \times (\mathbf{R}_{ib})^T\hat{\mathbf{k}}) \end{bmatrix} + \begin{bmatrix} \mathbf{F}_{ext} \\ \mathbf{T}_{ext} \end{bmatrix} \right\} \tag{32}$$

where $\mathbf{R}_{ib}$ is the rotation matrix that maps the body frame to the inertial frame.

Table 2 Estimated hydrodynamic coefficients of the ROUGHIE glider based on the Slocum glider [1]

Coefficient	Result	of	Value
K_D	Drag	force	25 kg/m/rad^2
K_{D0}	Drag	force	2.15 kg/m
K_L	Lift	force	132.5 kg/m/rad^2
K_{L0}	Lift	force	0 kg/m
K_β	Side	force	20 kg/m/rad
K_{MR}	Roll	moment	−6 kg/rad
K_p	Roll	moment	−20 kg/ s/rad
K_M	Pitch	moment	−100 kg/rad
K_{M0}	Pitch	moment	0 kg
K_q	Pitch	moment	−60 kg s/rad^2
K_{MY}	Yaw	moment	110 kg/rad
K_r	Yaw	moment	−20 kg s/rad^2

Spiraling motion of gliders is a steady state glide motion in three dimensions and has been studied extensively in [23] and [22]. We utilize a modified version of the previously mentioned formulation to account for the ROUGHIE's improved roll mechanism. The new rotary mass mechanism allows us to simplify the result by eliminating the position of the rotary mass in the formulation, since steady state motion only depends on the internal roll angle.

During the turn maneuver in ROUGHIE, the sliding mass travels to the feedforward position at $\mathbf{r}_s$ to induce the initial pitch angle, then the rotary servo pivots the common rail by γ to induce the yaw moment. We also assume that the rate of the buoyancy is zero ($\dot{m}_b = 0$) during the spiraling motion. To derive the equations of motion of the glider in the steady state we set $\dot{\boldsymbol{\nu}} = 0$ in Eq. 32, yielding

$$0 = \mathbf{P} \times \boldsymbol{\Omega} + m_b g(\mathbf{R}_{ib}^T \hat{\mathbf{k}}) + \mathbf{F}_{ext} \tag{33}$$

and

$$0 = \mathbf{Q} \times \boldsymbol{\Omega} + \mathbf{P} \times \mathbf{V} + (m_b \mathbf{r}_r + m_s \mathbf{r}_s + m_r \mathbf{r}_r) g \times (\mathbf{R}_{ib})^T \hat{\mathbf{k}}) + \mathbf{T}_{ext}. \tag{34}$$

We know that the glider speed in a circular helix is constant and the angular velocity is $\boldsymbol{\Omega} = \mathbf{R}_{ib}^T \omega_3 \hat{\mathbf{k}}$ [23], where ω_3 is the angular velocity of the glider along the circular helix. We denote the turn radius of the glider by R_t and express by

$$R_t = \frac{\|\mathbf{V}\| \cos(\theta - \alpha)}{\omega_3}. \tag{35}$$

In general, steady state spiraling motion can be characterized by 10 parameters according to [23]: V, α, β, ω_3, ϕ, θ, r_{rx}, γ, R_t, and net buoyancy. We have shown for our glider, however, that since steady state motion only depends on γ, r_{rx} is not needed to characterize its spiraling motion. We consider the scenario where we know the vehicle velocity parameters (V, α, and β), and we recognize that ω_3 is a function of θ and ϕ [23]. Since the net buoyancy is experimentally known, we simply must solve for ϕ, θ, and γ. To achieve the desired ϕ and θ the controller adjusts the roll servo rotation angle γ and the position of the sliding mass $\boldsymbol{r}_s$, respectively; the amount of the ballast is also another control input to achieve the desired pitch angle. The ROUGHIE utilizes a multi-layer controller [16] to navigate the glider in the mission area.

4 Navigation and Motion Control

In this section, we investigate the controller architecture derived from the kinematic model and refer to the dynamic model of the ROUGHIE. The controller, Fig. 4, interprets the desired trajectory into actionable desired attitude and velocity for the low-level controllers. The operation of this controller is discussed in detail in our previous work [16], in this work we extend its control capabilities to include roll and heading control.

The internally actuated and energy efficient design of the ROUGHIE places strict constraints on the speed and extent of actuation effort due to sizing and power constraints. As an internally actuated vehicle, control of the ROUGHIE relies on predictable coupling between actuation of $\mathbf{r}_s, m_b$, and γ to changes of z, θ, and ϕ for effective control. The glider kinematics described in Section 3 show that the internally actuated system in ROUGHIE predictably controls the glider dynamics. The navigational sensors used in the current configuration of ROUGHIE are an Attitude and Heading Reference System (AHRS), a pressure sensor, and two draw wire sensors. These sensors detect attitude (θ, ϕ, ψ), depth (z), amount of ballast (m_b), and sliding mass position ($\mathbf{r}_s$), respectively. Additional sensors are deployed on an as-needed basis.

The dive plane is the primary locomotive plane for underwater gliders as it contains both vertical and forward motion. In the ROUGHIE, depth (z) and pitch (θ) are governed by m_b. To initiate a glide, the buoyancy drive is actuated causing a net positive (or negative) buoyancy and the vehicle to rise (or fall) in the water column. The forward location of the ballast tank relative to the vehicle's center of buoyancy contributes a pitching moment such that the ROUGHIE trends towards the desired pitch angle (θ). Fine control of θ is achieved by updating $\mathbf{r}_s$. The buoyancy module and pitch module behavior is dictated by the control laws

$$u_z = sign(e_z) \tag{36}$$

$$u_\theta = k_{p_\theta} e_\theta + k_{i_\theta} \int_0^t e_\theta d\tau + k_{d_\theta} \dot{e}_\theta + w_0 \tan\theta, \tag{37}$$

where k_{p_θ}, k_{i_θ}, and k_{d_θ} are positive control gains, $e_z = z - \bar{z}$ and $e_\theta = \theta - \bar{\theta}$ are errors in the depth and pitch angle, respectively, and u_z and u_θ are control inputs to the buoyancy and pitch modules. Note that the term $w_0 \tan\theta$ is the feedforward part of the controller and depends on the initial vertical velocity

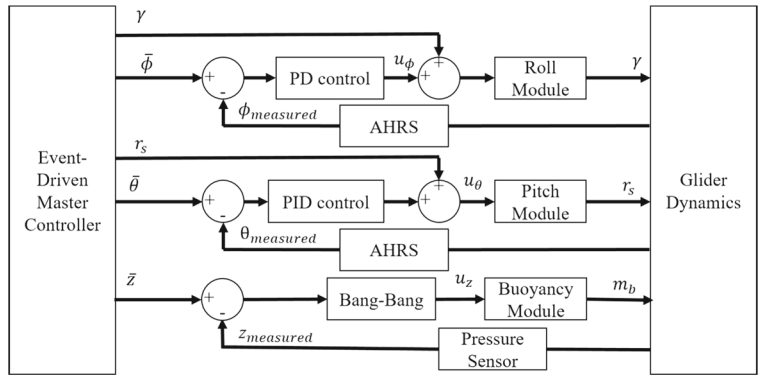

Fig. 4 Multi-layer control strategy used in ROUGHIE. The Event-Driven Master Controller interprets the desired trajectory into actionable pitch ($\bar{\theta}$), depth ($\bar{z}$), and roll ($\bar{\phi}$) targets for the low level controllers

and pitch angle; the amount of buoyancy determines the vehicle's initial velocity.

Motion control in the dive plane is achieved using a hybrid feedforward-feedback approach [12]. Since the ROUGHIE is restricted to operation in shallow water, the vehicle does not have enough depth or the appropriate time to achieve steady state using traditional feedback control. Thus, to initiate a glide, the hybrid approach uses the feedforward element to shift the ballast piston and sliding mass to predefined positions, accelerating vehicle convergence rate to the desired trajectory. Then, during steady glides the controller utilizes feedback to compensate for errors and improve performance.

As expected, the hybrid controller rapidly approaches the desired glide angle and is computationally affordable for a hobby level microprocessor. Pool deployment of the hybrid feedforward-feedback controller results in better pitch control as shown in Fig. 5. We use a switching control method in the transition segment between glide states. This switching approach toggles the feedback element of the hybrid controller off and the feedforward element drives the ROUGHIE to a neutrally buoyant state. As soon as the vehicle is in steady state the controller switches to hybrid control, thus driving to the desired trajectory for the next glide segment. Figure 6 illustrates the effect of switching control approach in a glide cycle.

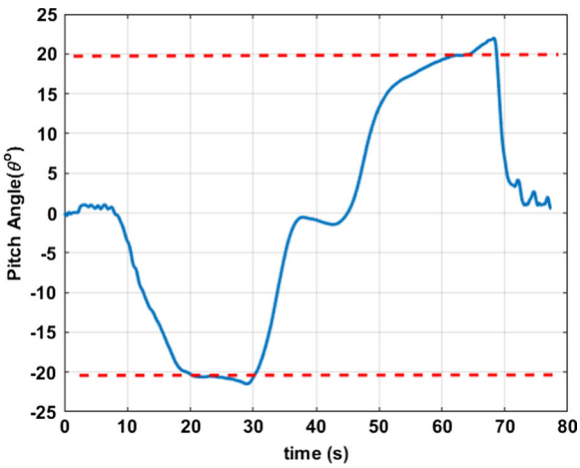

Fig. 5 The ROUGHIE pitch controller operates using a switching control approach. During glide segments, a hybrid feedforward-feedback controller enables rapid convergence to the target glide trajectory. The switching controller assumes a neutrally buoyant state between glide segments ($t \approx 40s$). Target pitch angles for this test were $\pm 20°$

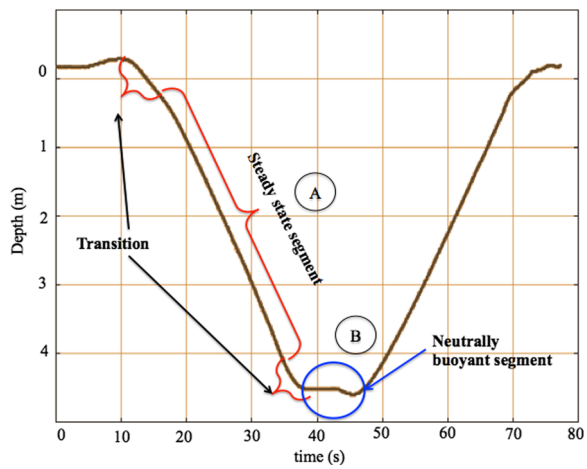

Fig. 6 During each glide cycle the ROUGHIE uses a switching control strategy depending on the current glide state. In segment (**A**) a hybrid feedforward-feedback controller is used. In segment (**B**) a neutrally buoyant state is commanded using feedforward control

The focus of this paper is the glider maneuverability, particularly with respect to turning motion. In underwater gliders, turning motion results from the combination of forward motion in the dive plane and change of heading in the lateral plane. Change in heading is achieved by rolling the vehicle, causing the wing's lift vector to rotate (ϕ). The vehicle dynamics then force the ROUGHIE into turning motion. The novel roll mechanism in ROUGHIE rotates all the vehicle internals around the longitudinal axis by γ which effectively shifts the vehicle's center of gravity in the direction of the lateral axis to achieve the desired roll angle $\bar{\phi}$. Roll control is achieved in two different ways in the ROUGHIE:

1) γ command is sent directly to the servo, or 2) γ command is obtained through feedback control of ϕ. Case 1 is used for either system identification or feedforward-based inverse mapping implementation. Case 2 control is used for long-term turn control, or if the system has not been properly characterized following changes to the vehicle structure. Case 2 control becomes,

$$u_\phi = k_{p_\phi} e_\phi + k_{d_\phi} \dot{e}_\phi \tag{38}$$

where desired roll angle ($\bar{\phi}$) is calculated by the master controller and $e_\phi = \phi - \bar{\phi}$.

In roll, the feedforward component is calculated based on the required turn radius and the feedback component is computed from feedback from the internal AHRS. The roll controller performs significantly better than the pitch controller as the roll module actuates the majority of the vehicle mass, has a faster actuator, and is dynamically decoupled from the other vehicle states. Using the switching controller the glider is able to link different maneuvers in a single mission. To successfully control the glider in 3D space, simultaneous control of both lateral plane and dive plane is required.

To calculate the trajectory of the ROUGHIE, the algorithm needs two sensory inputs, the pressure and attitude. The depth is determined by data provided from a pressure sensor and an AHRS provides the glider's pitch (θ), yaw (ψ), and roll (ϕ) angles. The following equations summarize the method used to calculate the position and speed of the glider at each time step.

$$w = -\frac{z_i - z_{i-1}}{\tan(\theta)} \tag{39}$$

$$u = w \cdot \sin(\psi) \tag{40}$$

$$v = w \cdot \cos(\psi) \tag{41}$$

$$\triangle(x) = u \cdot \triangle(t) \tag{42}$$

$$\triangle(y) = v \cdot \triangle(t) \tag{43}$$

$$x_{i+1} = x_i + \triangle(x) \tag{44}$$

$$y_{i+1} = y_i + \triangle(y) \tag{45}$$

The vertical position of the glider is derived by

$$\dot{z} = w \cdot \cos(\theta) + u \cdot \sin(\theta). \tag{46}$$

Thus, the position of the vehicle in 3D space is determined using the glider velocity and orientation at any moment, and the vertical position of the vehicle is validated using the depth sensor data.

5 Results

The ROUGHIE has been deployed on over 200 hours of basic systems characterization out of which 80 hours were dedicated to roll characterization and turning motion control. Presented here are results pertaining primarily to lateral plane motion undertaken at the Michigan Technological University Student Development Complex pool. The pool is 15.84 m long, 11.88 m wide and up to 4.27 m deep. The majority of the pool is less than 4.27 m deep as the pool floor is sloped like other diving wells. The small test area imposes additional constraints on the ROUGHIE motion as it is required to perform very tight maneuvers at shallow depth. These constraints increase the level of difficulty and introduce new challenges that mirror those that currently impede underwater glider use in hazardous underwater zones.

This section demonstrates the experimental validation results for the ROUGHIE turning capabilities and functionality. In Section 5.1 roll characterization relating γ to ϕ is presented. In Section 5.2 the turn motion and initial characterization of the transition between multiple turning flights are discussed.

5.1 Roll Characterization

To effectively characterize the roll system, a series of tests were conducted where the roll module's servo was driven to various γ angles between 20 and 70 degrees and the vehicle's dynamic roll response (ϕ) was measured using the internal AHRS. To perform this test, the ROUGHIE assumes a neutrally buoyant state underwater. Roll control then engages and rotates the ROUGHIE clockwise and counterclockwise multiple times to begin the characterization test. Based on the glider kinematics, roll motion is decoupled from dive plane motion and can be tested independently. Note this test must be performed at a depth where the wing will remain submerged throughout the various roll angles, eliminating any surface and air interactions on the roll response.

The results for pure feedforward roll control (Case 1), illustrated in Fig. 7, show that the ROUGHIE is able to effectively achieve various roll angles using the internal servo-based roll mechanism, and can achieve a roll in excess of 60 degrees. Note that in some cases the roll response shown in Fig. 7 is not symmetric about 0 degrees, which is an artifact of the trimming weights added to the ROUGHIE instead of the scientific payload. While these weights were manually arranged as symmetrically as possible, there is some inherent error in their placement.

As an additional characterization of the roll system, we completed the same experiment with the hybrid feedforward-feedback roll controller (Case 2). Figure 8 shows the resulting vehicle roll angles. The addition of feedback control to the roll controller compensates for the presence of asymmetric trim weight. Comparing Figs. 7 and 8, the hybrid controller is able to achieve the target vehicle roll (ϕ) up to approximately 50°.

5.2 Roll Controller Effect on Turning Motion

The spatial constraints of the swimming pool prohibit testing of spiraling motion, therefore to evaluate the ROUGHIE's capability to perform spiraling motion

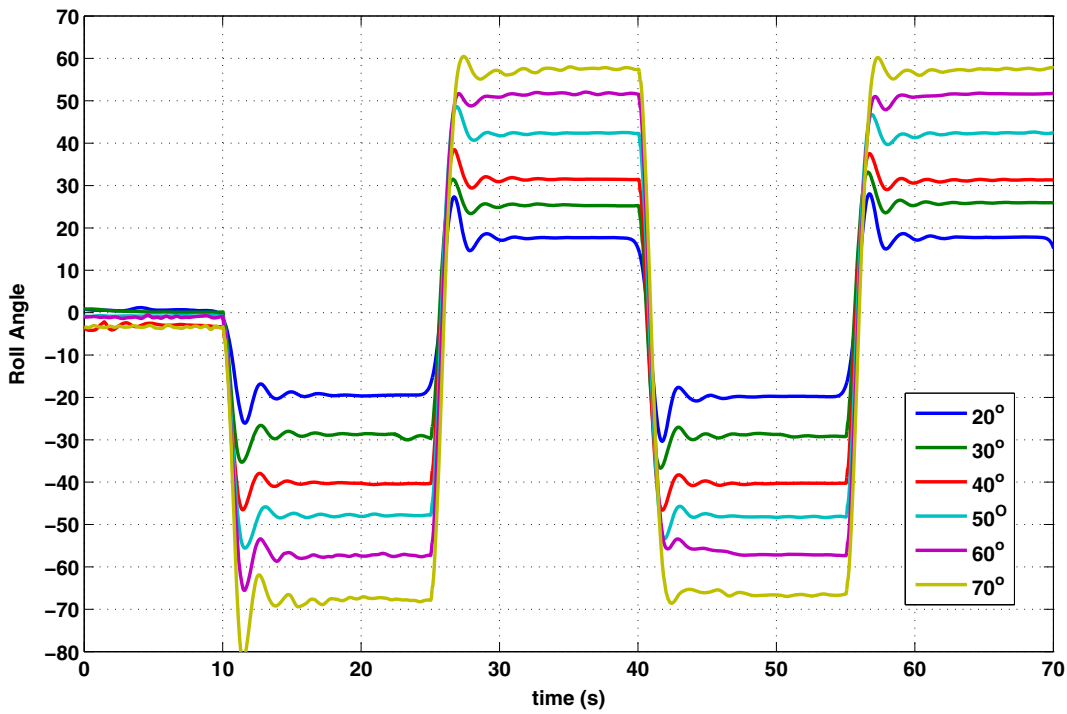

Fig. 7 ROUGHIE roll response (ϕ) to commanded servo roll angle (γ), pure feedforward (Case 1) control. The dynamic response in vehicle roll angle is recorded using an AHRS sensor. As shown the system rapidly approaches a steady state roll angle that is slightly less than the internal servo angle due to the trimming method used

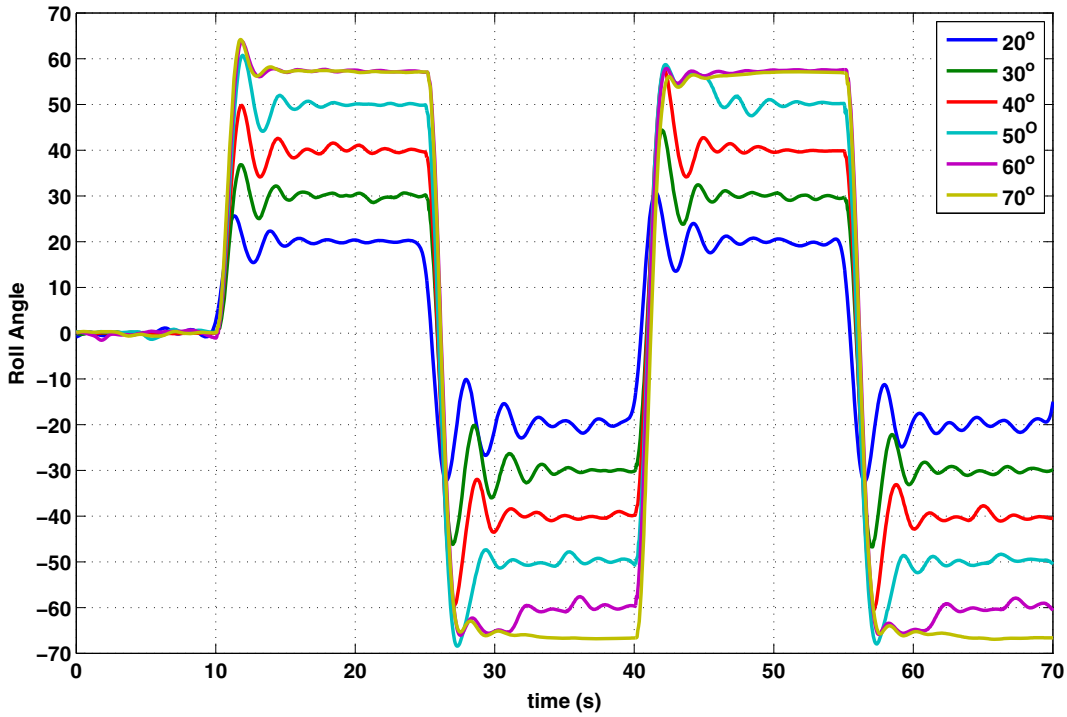

Fig. 8 ROUGHIE roll response using to commanded ϕ using the feedforward-feedback (Case 2) control. The controller is capable of maintaining accurate roll angles through natural disturbances

we implemented a *turn around a point* maneuver as concatenation of steady flights using switching control approach discussed in Section 4. In this experiment, as depicted in Fig. 9a and b, the ROUGHIE performs three concatenated motions (spiral down, neutrally buoyant, spiral up) in each glide cycle.

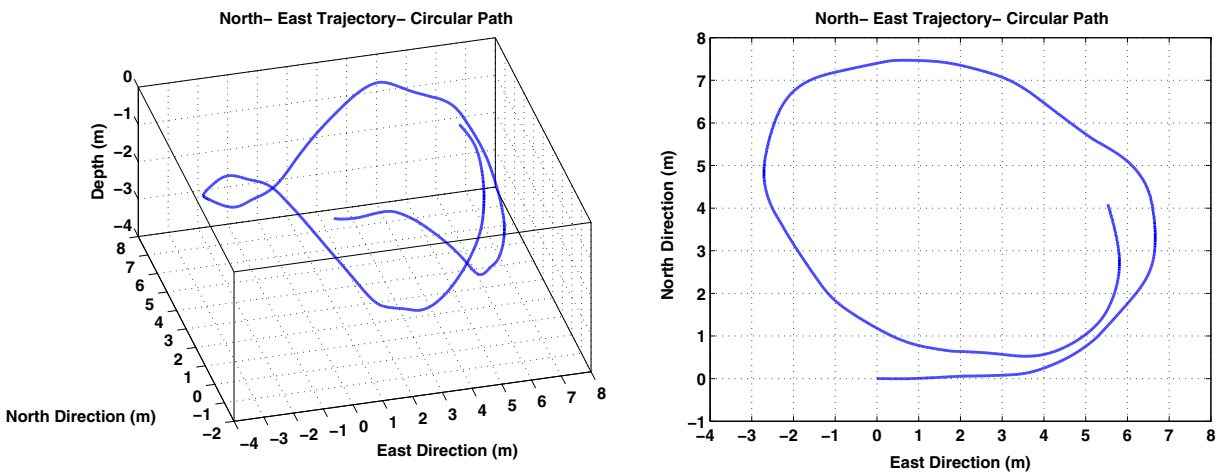

(a) 3D view **(b)** top view

Fig. 9 The ROUGHIE completes a turn around a point maneuver by performing three concatenated motions (spiral down, neutrally buoyant, spiral up). The full circle is achieved in two glide cycles

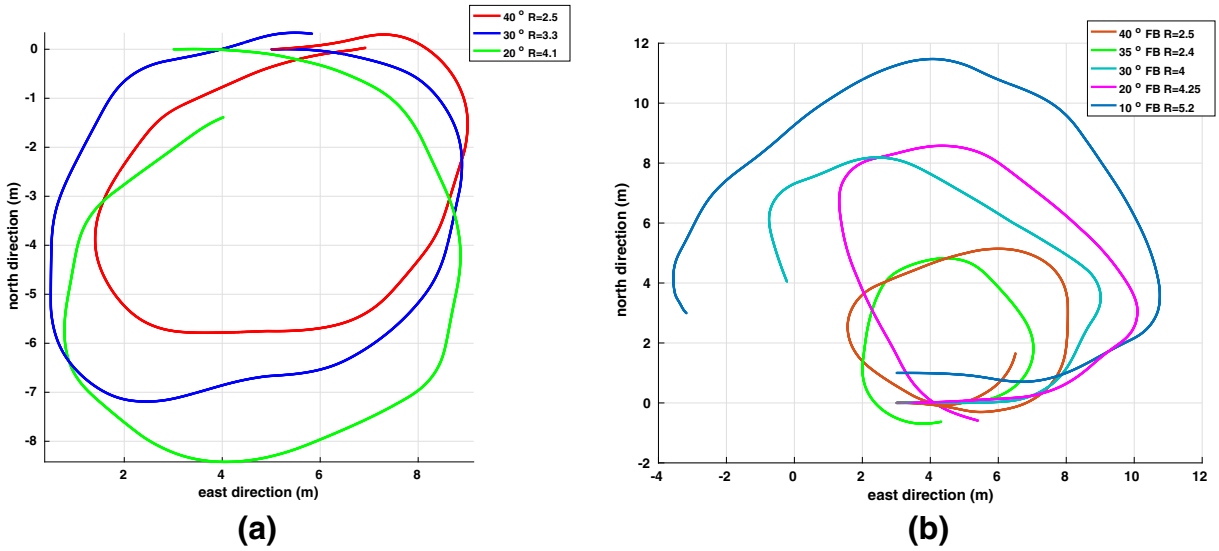

Fig. 10 The ROUGHIE deployed on concatenated turning missions at various roll angles in restricted water with maximum depth of 3 meters. The vehicle is capable of linking multiple turns on successive glides into one cohesive circular motion. (**a**) Feedforward control (Case 1) (**b**) Hybrid control (Case 2)

At the beginning of the turn around a point motion, the ROUGHIE rolls to a desired roll angle, then by change of buoyancy and feedforward position of the sliding mass the vehicle enters the glide down cycle. Since the vehicle is banked, the effect of hydrodynamic forces induces a change of heading and the glider enters a circular trajectory and turns. The motion is continued until it is near the desired depth when the controller then levels the glider and enters the neutrally buoyant state to temporarily create an equilibrium point. At this point the ROUGHIE has traveled through approximately 90° arc of the circle. Next, the ROUGHIE then enters the glide up stage by rolling to the opposite side, pushing the sliding mass to a new location, and entering the positively buoyant state. The glider continues its motion to complete a half circle in one glide cycle.

To complete a full circle, the ROUGHIE performs two glide cycles and returns back to the home position. The tightest circle performed has a 2.4 meter radius for the 1.2 meter ROUGHIE with a roll angle of 35°. The experimental trajectories illustrated in Fig. 10 show that the roll angle has an inverse relationship with the vehicle's turn radius. While performing smaller roll angles, the circle radius becomes larger and it takes longer time to complete the circle. Thus, an extra glide cycle has to be added when using roll angles less than 30° to complete a full 360° turn.

6 Conclusion and Future Work

In this paper an effective turning motion control strategy is presented for internally actuated underwater gliders. The proposed roll mechanism and controller have been experimentally validated on Michigan Tech's research underwater glider, making the ROUGHIE extremely maneuverable compared to existing underwater gliders by increasing its capability in turn motion.

The roll mechanism is of a novel design that utilizes the vast majority of vehicle mass as eccentric control mass mounted on a common rail. By actuating the common rail, the ROUGHIE is capable rolling in excess of 60° in a short amount of time. The vehicle hydrodynamics combined with the large roll angle results in tight turn radius down to 2.4 meters for a 1.2 meter long vehicle while operating in shallow water. The vehicles capability of linked steady glides is validated through the completion of a circular motion profile in less than 3 meters of water in a controlled swimming pool environment.

With the ROUGHIE turning mechanism well characterized, we will be expanding our work into complex path following, navigation, autonomous operation, and operation at deeper depths. Our future work will initially focus on linking multiple steady glides to create optimal paths between way points and performing heading control. We will then integrate additional sensors such as a velocity probe for aided dead reckoning, a forward looking sonar for obstacle avoidance, and intelligent navigation. Multi-vehicle testing is also beginning as we start looking at fleet control and optimization for long endurance area coverage missions. ROUGHIE is highly maneuverable and flexible in its modular design, making it easy to modify hardware and software, and therefore, serving the purpose of different research groups who need to experiment with and validate control algorithms.

References

1. Abraham, I., Yi, J.: Model Predictive Control of Buoyancy Propelled Autonomous Underwater Glider. In: 2015 American Control Conference (ACC), pp. 1181–1186. IEEE (2015)
2. Allotta, B., Costanzi, R., Ridolfi, A., Colombo, C., Bellavia, F., Fanfani, M., Pazzaglia, F., Salvetti, O., Moroni, D., Pascali, M.A., et al: The arrows project: adapting and developing robotics technologies for underwater archaeology. IFAC-PapersOnLine **48**(2), 194–199 (2015)
3. Alvarez, A., Caffaz, A., Caiti, A., Casalino, G., Gualdesi, L., Turetta, A., Viviani, R.: Folaga: a low-cost autonomous underwater vehicle combining glider and auv capabilities. Ocean Eng. **36**(1), 24–38 (2009)
4. Anderson, B., Crowell, J.: Workhorse AUV– a cost-sensible new autonomous underwater vehicle for surveys/soundings, search & rescue, and research. In: Proceedings of OCEANS 2005 MTS/IEEE. Institute of Electrical & Electronics Engineers (IEEE). doi:10.1109/oceans.2005.1639923
5. Bhatta, P., Leonard, N.E.: Nonlinear gliding stability and control for vehicles with hydrodynamic forcing. Automatica **44**(5), 1240–1250 (2008). doi:10.1016/j.automatica.2007.10.006
6. Cao, J., Cao, J., Yao, B., Lian, L.: Dynamics and adaptive fuzzy turning control of an underwater glider. In: OCEANS 2015 - Genova. Institute of Electrical & Electronics Engineers (IEEE) (2015). doi:10.1109/oceans-genova.2015.7271363
7. Eriksen, C., Osse, T., Light, R., Wen, T., Lehman, T., Sabin, P., Ballard, J., Chiodi, A.: Seaglider: a long-range autonomous underwater vehicle for oceanographic research. IEEE J. Ocean. Eng. **26**(4), 424–436 (2001). doi:10.1109/48.972073
8. Fan, S., Wolek, A., Woolsey, C.A.: Stability and performance of underwater gliders. In: 2012 Oceans, pp. 1–10 (2012). doi:10.1109/OCEANS.2012.6404993
9. Fossen, T.I.: Handbook of marine craft hydrodynamics and motion control John Wiley & Sons (2011)
10. Kan, L., Zhang, Y., Fan, H., Yang, W., Chen, Z.: MATLAB-based simulation of buoyancy-driven underwater glider motion. J. Ocean Univ. China **7**(1), 113–118 (2008). doi:10.1007/s11802-008-0113-2
11. Leonard, N., Graver, J.: Model-based feedback control of autonomous underwater gliders. IEEE J. Ocean. Eng. **26**(4), 633–645 (2001). doi:10.1109/48.972106
12. Mahmoudian, N., Woolsey, C.: Analysis of feedforward/feedback control design for underwater gliders based on slowly varying systems theory. In: AIAA Guidance, Navigation, and Control Conference. American Institute of Aeronautics and Astronautics (AIAA) (2009). doi:10.2514/6.2009-5755
13. Page, B.R., Ziaeefard, S., Pinar, A.J., Mahmoudian, N.: Highly maneuverable low-cost underwater glider: Design and development. IEEE Robotics and Automation Letters **2**(1), 344–349 (2017). doi:10.1109/LRA.2016.2617206
14. Philips, A., Steenson, L., Rogers, E., Turnock, S., Harris, C., Furlong, M.: Delphin2: an over actuated autonomous underwater vehicle for manoeuvring research. Transactions of the Royal Institution of Naval Architects, Part A–International Journal of Maritime Engineering **155**(A4), 171–180 (2013)
15. Ribas, D., Ridao, P., Turetta, A., Melchiorri, C., Palli, G., Fernandez, J.J., Sanz, P.J.: I-AUV mechatronics integration for the TRIDENT FP7 project. IEEE/ASME Trans. Mechatron. **20**(5), 2583–2592 (2015). doi:10.1109/tmech.2015.2395413
16. Ribeiro, G.A., Pinar, A., Wilkening, E., Ziaeefard, S., Mahmoudian, N.: A multi-level motion controller for low-cost underwater gliders. In: 2015 IEEE International Conference on Robotics and Automation (ICRA). Institute of Electrical & Electronics Engineers (IEEE) (2015). doi:10.1109/icra.2015.7139333
17. Rusling, M.: Gliders will aid naval research National Defense Industrial Association Business and Technology Magazine (2009)
18. Shen, Y., Hu, P., Jin, S., Wei, Y., Lan, R., Zhuang, S., Zhu, H., Cheng, S., Chen, J., Wang, D., Liu, D.: Design of novel shaftless pump-jet propulsor for multi-purpose long-range and high-speed autonomous underwater vehicle. IEEE Trans. Magn. **52**(7), 1–4 (2016). doi:10.1109/TMAG.2016.2522822
19. Sherman, J., Davis, R., Owens, W., Valdes, J.: The autonomous underwater glider spray. IEEE J. Ocean. Eng. **26**(4), 437–446 (2001). doi:10.1109/48.972076

20. Teledyne: Teledyne webb research reaches second milestone with u.s. navy lbs-glider program. http://www.webbresearch.com/newscenter/Reaches_Second_Milestone.aspx (2011)
21. Webb, D., Simonetti, P., Jones, C.: SLOCUM: an underwater glider propelled by environmental energy. IEEE J. Ocean. Eng. **26**(4), 447–452 (2001). doi:10.1109/48.972077
22. Zhang, F., Zhang, F., Tan, X.: Tail-enabled spiraling maneuver for gliding robotic fish. J. Dyn. Syst. Meas. Control. **136**(4), 041,028 (2014). doi:10.1115/1.4026965
23. Zhang, S., Yu, J., Zhang, A., Zhang, F.: Spiraling motion of underwater gliders: Modeling, analysis, and experimental results. Ocean Eng. **60**, 1–13 (2013). doi:10.1016/j.oceaneng.2012.12.023
24. Zhang, Y., Bellingham, J.G., Ryan, J.P., Kieft, B., Stanway, M.J.: Autonomous four-dimensional mapping and tracking of a coastal upwelling front by an autonomous underwater vehicle. J. Field Rob. **33**(1), 67–81 (2015). doi:10.1002/rob.21617
25. Ziaeefard, S., Page, B.R., Pinar, A.J., Mahmoudian, N.: A novel roll mechanism to increase maneuverability of autonomous underwater vehicles in shallow water. In: OCEANS 2016 MTS/IEEE Monterey, pp. 1–5 (2016). doi:10.1109/OCEANS.2016.7761160

Saeedeh Ziaeefard received a M.S. degree from Amirkabir University of Technology, Tehran, Iran in 2007. She has five years of work experience in shipbuilding and offshore engineering. She is currently a Ph.D. candidate in the Department of Mechanical Engineering-Engineering Mechanics at Michigan Tech. Her research interest include autonomous underwater vehicles, controls, path planning and underwater navigation.

Brian R. Page received a M.S. degree from Michigan Technological University in 2016. He is currently a Ph.D. student in the Department of Mechanical Engineering-Engineering Mechanics at Michigan Tech. His research interests include autonomous systems, controls, and mechanical design.

Anthony J. Pinar received a M.S. degree from Michigan Technological University, Houghton, MI in 2014. He is currently a Ph.D. candidate in the Department of Electrical and Computer Engineering at Michigan Tech. His research interests include autonomous underwater robots, machine learning, computational intelligence, and signal/image processing.

Nina Mahmoudian received her Ph.D. in aerospace engineering from Virginia Polytechnic and State University (Virginia Tech), Blacksburg, VA, in 2009. She is an Assistant Professor at the Department of Mechanical Engineering-Engineering Mechanics, Michigan Technological University (Michigan Tech), Houghton, MI. Dr. Mahmoudian is the founding director of Nonlinear and Autonomous Systems Lab (NAS Lab). Her research interests include cyber physical systems, dynamics and control of autonomous systems, and energy autonomy. Dr. Mahmoudian is a recipient of 2015 National Science Foundation (NSF) CAREER Award and 2015 U.S. Office of Naval Research (ONR) Young Investigator Program (YIP) Award.